34th Symposium on Naval Hydrodynamics
Washington, DC, USA, 26 June -1 July 2022

Multi-Fidelity Uncertainty Quantification and Reduced-Order Modeling for Extreme Ship Motions and Loads

V. Pipiras[1], D. Howard[2], V. Belenky[3], K. Weems[3] and T. Sapsis[2]
([1]University of North Carolina at Chapel Hill, USA [2]Massachusetts Institute of Technology, USA [3]Naval Surface Warfare Center, Carderock Division (NSWCCD), Maryland, USA)

ABSTRACT

The paper has two major components. How data from two multi-fidelity (MF) sources can be combined to estimate extreme quantities for higher-fidelity source is the first component. The better MF source outputs are calibrated, the more successful these methods are in reducing the size of confidence intervals in statistical uncertainty quantification (UQ). Calibrating computer codes of different fidelities and computational efficiencies for ship motions and loads, with the focus on their extremes, is the second component. A physics-based approach involving regressions of forces is evaluated, whereas a neural network, namely, the long short-term memory (LSTM) model, is another. The data generated by the codes serve to show the feasibility of the proposed MFUQ methods, with the LSTM holding greatest promise for code calibration.

INTRODUCTION

Multi-fidelity (MF) methods and statistical uncertainty quantification (UQ) are described for extremes of ship motions and (wave-induced) loads. Extreme ship motions are associated with pure loss of stability, surf-riding and broaching, and other dangerous conditions. Extreme loads could lead to ship's structural damage. Randomness throughout this work results from random (irregular) ocean waves. The MF data sources are several computer codes for ship motions. In fact, a range of such computer codes are employed in the Naval Architecture community and can differ substantially in their fidelity and computational efficiency. But if the codes produce comparable outputs, perhaps after additional tuning or suitable "mapping," the data from a lower-fidelity code could help in estimating extreme quantities for a high-fidelity code. Several methods for achieving this task are presented. Calibration of ship motion codes is evaluated through suitable tuning of coefficients and "mapping." The described methods should be useful not only in the context of ship motions but also in other situations, where data are available from MF sources and extremes are of interest.

Two MF-like computer codes for ship motions and loads are presented: Large Amplitude Motion Program (LAMP), on one hand, and SimpleCode (SC) and related reduced-order ordinary differential equation (ODE) models, on the other hand. The higher-fidelity LAMP solves a wave-body interaction problem in the time domain via a 3-dimensional potential flow panel method and has a number of other characteristics and options (Lin and Yu [9], Shin et al. [14]). The lower-fidelity but computationally more efficient SC and similar reduced-order models solve ODE systems with added mass and damping coefficients that capture radiation forces acting on a ship, while incorporating the non-linear Froude-Krylov and hydrostatic (FKHS) forces through a volume-based calculation of the submerged hull rather than integration of pressures (Weems and Wundrow [17]). More details on these codes can be found below. As a way of calibrating SC and related codes, a physics-informed approach is discussed based on regression of forces, extending earlier work from regular to irregular waves (Pipiras et al. [12]). The calibration here will consider motions only but could be readily extended to loads. Methods are examined for mapping SC motions and loads to those of LAMP through long-short term memory (LSTM) neural networks. The LSTM model also appears in a parallel work in the proceedings (Levine et al. [8]) but extreme outputs are the focus here.

On the data, extremes and UQ front, typical LAMP and SC outputs are 30-minute records of ship motions and (wave-induced) loads, that can be obtained on the same wave excitation. Wave excitation is characterized by a record number, which plays the role of a random seed for generating phases in generating specific realizations of ocean waves from a theoretical

or experimental spectrum. Given motion or load outputs, various extreme value type questions could be asked. For example, the record maximum (for some motion or load) can be computed and reviewed across multiple records, for both LAMP and SC. For multiple record maxima, a generalized extreme value distribution (GEVD) could be fit to data, and then applied for extrapolation into the regions with no data (e.g. Coles [4]). Any such extrapolation requires statistical UQ through confidence intervals. How these confidence intervals could potentially be reduced when employing MF data is addressed. Record maxima and GEVD is just one possible setting of the applicability of this approach. The related discussion simplifies and reformulates the more methodological and technical presentation found in Brown and Pipiras [3].

The UQ setting above concerns MF data from a set of randomly selected records, referred to as "random sampling." In the context of LAMP and SC, a different "importance sampling" procedure for records can be performed. Here, a large number of SC records could be generated quickly first, and then LAMP records could be generated only for selective SC records, for example, those that have larger extreme values themselves. How uncertainty is quantified in this setting, and how estimators of extreme quantities are defined are some of the questions addressed in this work. The approach builds on similar questions for probability density function (PDF) estimation found in O'Connor et al. [10]. The MFUQ is related to several works cited below but their focus has generally been on non-extreme behavior. Studying extreme behavior is expected naturally to be more challenging.

PRELIMINARIES

LAMP, SC and reduced-order models

More information is provided on LAMP, SC, and related models. For simplicity but also for reference below, the case of head seas (ship pointing into the waves) is considered, resulting in heave ζ_g and pitch θ motions. In LAMP, the equations of motion are expressed as

$$\begin{cases} m\ddot{\zeta}_g = F_{3,fkhs} + F_{3,hd} \\ I_Y\ddot{\theta} = F_{5,fkhs} + F_{5,hd} \end{cases} \tag{1}$$

where m is the ship mass and I_Y is the pitch mass moment of inertia, $F_{i,fkhs}$ and $F_{i,hd}$, $i = 3,5$, denote the respective FKHS and hydrodynamic force components. A general set of equations of motion, with the additional dependence on a coordinate system, can be found, for example, in Weems et al. [15].

Various versions of LAMP are available depending on how forces in (1) are computed, as summarized in the following table:

LAMP-2	3-D body-nonlinear method
LAMP-1	body-linearized 3-D method
LAMP-0	"Hydrostatics only" formulation

LAMP-2 incorporates a body-nonlinear formulation for FKHS, while hydrodynamic forces are resolved over the mean waterline, i.e. are linearized. LAMP-1 incorporates a body-linear formulation for FKHS and body-linear solution for hydrodynamic forces. LAMP-0 is a capability to switch off the hydrodynamic solver, either for body linear or body nonlinear formulation for FKHS, with the option for coefficient representation for hydrodynamic forces. More details are in Weems et al. [16]. The calculations marked LAMP below will be for LAMP-2, unless stated otherwise.

The hydrodynamic forces in (1) include radiation and diffraction forces, that is,

$$F_{i,hd} = F_{i,rad} + F_{i,dif}. \tag{2}$$

This decomposition holds only without the nonlinear term in the Bernoulli equation. The latter is an option in LAMP, among many other available options. LAMP also has the capability to output various forces and other quantities of interest, do calculations for prescribed motions and fixed body, and so on.

The potential flow computation of the hydrodynamic forces makes LAMP computationally rather expensive. Reduced-order ODE models typically simplify the effect of radiation forces to a set of added mass and damping coefficients. For SC, these are the coefficients A_{ij} and B_{ij} in the system of equations:

$$\begin{cases} (m+A_{33})\ddot{\zeta}_g + A_{35}\ddot{\theta} + B_{33}\dot{\zeta}_g + B_{35}\dot{\theta} = F_3(\zeta_g,\theta,t) \\ (I_Y+A_{55})\ddot{\theta} + A_{53}\ddot{\zeta}_g + B_{53}\dot{\zeta}_g + B_{55}\dot{\theta} = F_5(\zeta_g,\theta,t) \end{cases} \tag{3}$$

where F_3 and F_5 are the FKHS forces. The effect of the diffraction forces is not taken into account in the equations (3). Further simplifications could be made in separating restoring and excitation in the FKHS forces. The choice of the coefficients A_{ij}, B_{ij} is often ad hoc but driven by simulation experience. A physics-informed regression-based approach to choose them is presented below.

If producing a 30-minute record for SC takes a few seconds, the same task can take hundreds times longer for LAMP.

Dealing with loads is generally considered more challenging than motions (as the former are associated with forces, whereas the latter with their integration). Two other parallel papers in the proceedings (Belenky et al. [1], Sapsis et al. [13]) are related to reduced-order models for loads.

Ship geometry

The simulations presented below will be for the flared variant of the ONR Topsides Geometry Series (Bishop et al. [2]), Figure 1. The operating (speed, heading) and sea state conditions will vary across the illustrations. For example, the illustrations for MFUQ methods below are in head seas, sea state 8 (with a significant wave height of 11.5 m, and a modal period of 16.4 sec) and speed of 10 kts. The heave and pitch motions for LAMP and SC in these conditions over a period of time are depicted in Figure 2.

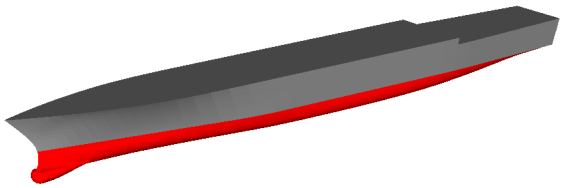

Figure 1: The ONR topsides flared geometry.

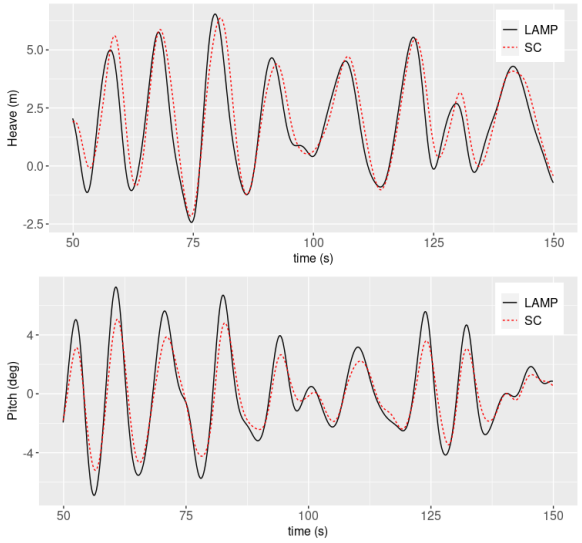

Figure 2: The heave and pitch motions for LAMP and SC.

Extremes, quantities of interest and UQ

Extreme behavior of ship motions and loads is discussed. A typical quantity of interest is an exceedance probability

$$\mathbb{P}(X > x^*) =: p(x^*), \tag{4}$$

where x^* is some critical exceedance value and X is a random variable of interest. The variable X could be a motion or load itself, or some extreme quantity thereof such as record maximum, suitable peak value, etc. For illustration purposes, X will typically be a record extreme (maximum or minimum). To estimate the probability $p(x^*)$ with UQ is the goal given a finite sample $X_1,\ldots,X_n$. To provide estimates and UQ over a range of values x^* is a related more ambitious goal.

The critical value x^* need not to be in the range of the sample $X_1,\ldots,X_n$ to estimate the probability (4). But what is needed is a PDF $f_\eta(x)$ of X where η is a (vector) parameter so that an estimate of (4) could be taken as

$$\widehat{p}(x^*) = \int_{x^*}^{x_u} f_{\widehat{\eta}}(x)dx, \tag{5}$$

where $\widehat{\eta}$ estimates η based on the sample, and x_u is the maximum X value (possibly infinity). That is, the estimated PDF $f_{\widehat{\eta}}(x)$ is used to extrapolate into the domain $x > x^*$. The choice of f_η can be motivated by a physical understanding of the system, or driven by the choice of X. For example, when X is a record extreme, the statistical extreme value theory allows to approximate its distribution by GEVD. This and other examples are considered below. If x^* falls in the range of the sample, the probability (4) could be expected to be estimated directly through a suitable average.

As estimation is based on a finite sample, $\widehat{\eta}$ and hence $\widehat{p}(x^*)$ are characterized by statistical uncertainty. The associated UQ is typically expressed through a confidence interval, and part of this work concerns such UQ issues. In view of (5), the uncertainty for $\widehat{\eta}$ propagates to that for $\widehat{p}(x^*)$. Several methods could be applied for such uncertainty propagation (e.g. Glotzer et al. [5]). One simple but more conservative method is a "boundary method." More specifically, if $\eta = (\eta_1,\ldots,\eta_d)$ consists of d univariate parameters and each comes with its confidence interval $(\widehat{\eta}_{k,l},\widehat{\eta}_{k,u})$, $k = 1,\ldots,d$ (l stands for "lower" and u for "upper" boundaries) with suitable adjusted confidence levels, uncertainty is propogated as

$$\widehat{p}_l(x^*) = \min_{b_k=l,u} \int_{x^*}^{x_u} f_{(\widehat{\eta}_{1,b_1},\ldots,\widehat{\eta}_{d,b_d})}(x)dx \tag{6}$$

for the lower boundary of the confidence interval for $p(x^*)$, and similarly for the upper boundary $\widehat{p}_u(x^*)$ with min replaced by max in (6). Another approach below is based on bootstrap. When the excedance probability is estimated directly through averages, simpler UQ methods are usually available.

MF setting and notation

In the introduction, an MF setting is of interest, where outputs are available from two related codes. Following the notation above, $X^{(1)}$ refers to the variable of interest for higher-fidelity code (e.g., LAMP), and $X^{(2)}$ to that for lower-fidelity code (e.g., SC). A sample $(X_i^{(1)},X_i^{(2)})$, $i = 1,\ldots,n_1$, of $(X^{(1)},X^{(2)})$ is available. In the ship application, $(X^{(1)},X^{(2)})$ are

obtained under the same random wave excitation. Two types of scenarios for obtaining the sample will be considered below: random sampling and importance sampling. Additional observations $X_i^{(2)}$, $i = n_1 + 1, \ldots, n_1 + n_2$, from the lower-fidelity code are available, and availability presupposes that the lower-fidelity code is computationally more efficient. This is the case for SC over LAMP as noted above.

Using superscripts $^{(1)}$ and $^{(2)}$ shall continue to refer to the quantities associated with the respective two codes. When no confusion exits, these labels shall be applied as subscripts as well. For example, $p^{(1)}(x_1^*)$ will refer to the exceedance probability $\mathbb{P}(X^{(1)} > x_1^*)$, $f^{(2)}(x_2)$ to the PDF of $X^{(2)}$, etc.

The most basic problem addressed in this work is how the data on the lower-fidelity variable $X^{(2)}$ can help in estimating extreme quantities, e.g. $p^{(1)}(x_1^*)$, for the higher-fidelity variable $X^{(1)}$. The stronger the outputs of the two codes are dependent, the more the lower-fidelity data can reduce statistical estimation uncertainty for quantities of $X^{(1)}$. The latter motivates the issues addressed below behind better calibration of low-fidelity reduced-order models.

MFUQ FOR EXTREMES

Using the notation above is continued, and estimating $p^{(1)}(x_1^*)$ is of interest. Two different setting are considered, random and importance samplings, depending on how the lower-fidelity and higher-fidelity variables $X^{(1)}$ and $X^{(2)}$ are sampled.

Random sampling

Random sampling is a more traditional setting where $(X_i^{(1)}, X_i^{(2)})$, $i = 1, \ldots, n_1$, are obtained through random sampling of $(X^{(1)}, X^{(2)})$, and similarly for $X_i^{(2)}$, $i = n_1 + 1, \ldots, n_1 + n_2$. For example, if X's are record maxima, these would be obtained from the first $n_1 + n_2$ selected records (characterized by random seeds). As above, $X^{(1)}$ follows the parametric PDF $f_{\eta^{(1)}}(x_1)$, where $\eta^{(1)} = (\eta_1^{(1)}, \ldots, \eta_d^{(1)})$ is a (vector) parameter. Furthermore, the $\eta_k^{(1)}$'s can be expressed as suitable moments,

$$\eta_k^{(1)} = \mathbb{E}h_k(X^{(1)}),\ k = 1, \ldots, d, \tag{7}$$

for functions h_k. E.g., the pth moment arises with $h(x) = x^p$, but other functions h_k shall be specified.

The setting (7) is assumed for convenience, including the possibility of replacing the expected value by suitable averages, the computational efficiency of the resulting moment estimators, and the MF construction below. The moment estimator of (7) shall be denoted by

$$\overline{h_k(X^{(j)})} = \text{average of } \{h_k(X_i^{(j)})\}_i,$$

for both $j = 1$ and $j = 2$. Furthermore, to indicate the dependence on the sample considered, the subscript n_1 shall be added, when the sample $X_1^{(1)}, \ldots, X_{n_1}^{(1)}$ or $X_1^{(2)}, \ldots, X_{n_1}^{(2)}$ is employed, and n_2 when $X_{n_1}^{(2)}, \ldots, X_{n_1+n_2}^{(2)}$ is used. Thus,

$$\overline{h_k(X^{(1)})}_{n_1},\ \overline{h_k(X^{(2)})}_{n_1},\ \overline{h_k(X^{(2)})}_{n_2}. \tag{8}$$

E.g., $\overline{h_k(X^{(2)})}_{n_2} = \frac{1}{n_2}\sum_{i=n_1+1}^{n_1+n_2} h_k(X_i^{(2)})$. As with all moment-like estimators, they are unbiased implicitly, i.e.,

$$\mathbb{E}\overline{h_k(X^{(j)})}_n = \mathbb{E}h_k(X^{(j)})\ (= \eta_k^{(1)} \text{ if } j = 1), \tag{9}$$

for any sample size n. This is an important property, when defining MF estimtors below.

Example: (Zero-mean Gaussian distribution.) If $f_{\eta^{(1)}}(x_1)$ is a zero-mean Gaussian PDF, then $\eta_1 = \sigma^2$ is the variance and, with zero mean, also the second moment, so that

$$\eta_1 = \sigma^2, \quad \overline{(X^2)}_n = \frac{1}{n}\sum_{i=1}^{n} X_i^2. \tag{10}$$

This model is suitable for centered motions and loads in a linear regime, typically associated with smaller to moderate waves. The next example is the focus.

Example: (Generalized extreme value distribution.) GEVD arises as the limiting distribution of extrema of a collection of variables, e.g. record maxima in the application, e.g., Coles [4]. The cumulative distribution function (CDF) of GEVD is given by

$$F(x) = \begin{cases} \exp\Big\{-(1+\gamma\frac{x-\mu}{\sigma})^{-1/\gamma}\Big\}, & \text{if } 1+\gamma\frac{x-\mu}{\sigma} > 0, \\ & \gamma \neq 0, \\ \exp\Big\{-\exp\{-\frac{x-\mu}{\sigma}\}\Big\}, & \text{if } \gamma = 0, \end{cases} \tag{11}$$

and is characterized by a location parameter μ, a scale parameter σ, and a shape parameter γ. Alternatively, the parametrization could also be expressed through the three, so-called L-moments,

$$\beta_r = \mathbb{E}(XF(X)^r),\ r = 1, 2, 3, \tag{12}$$

which relate to μ, σ, γ through

$$\begin{cases} \beta_0 = \mu - \dfrac{\sigma}{\gamma}(1 - \Gamma(1-\gamma)) \\ 2\beta_1 - \beta_0 = \dfrac{\sigma}{\gamma}\Gamma(1-\gamma)(2^\gamma - 1) \\ \dfrac{3\beta_2 - \beta_0}{2\beta_1 - \beta_0} = \dfrac{3^\gamma - 1}{2^\gamma - 1} \end{cases} \tag{13}$$

(Hosking et al. [7]). The unbiased estimators (i.e. satisfying (9)) of β_r are

$$\widehat{\beta}_r = \overline{(XF(X)^r)}_n = \frac{1}{n}\sum_{i=1}^{n}\Big(\prod_{\ell=1}^{r}\frac{i-\ell}{n-\ell}\Big)X_{i,n}, \tag{14}$$

where $X_{1,n} \leq \ldots \leq X_{n,n}$ represents the ordered GEV distributed sample. The GEVD is assumed for the PDF $f_{\eta^{(1)}}(x_1)$.

Other examples that can be considered include Weibull distribution, Gumbell distribution, generalized Pareto distribution, and so on.

The higher-fidelity PDF $f_{\eta^{(1)}}(x_1)$ parameter $\eta^{(1)}$ can potentially be estimated with less uncertainty when taking advantage of the availability of lower-fidelity data. Then, the uncertainty propagated onto e.g. exceedance probability $p^{(1)}(x_1^*)$ through (5) would also be expected to be smaller. More specifically, for moment parameters (7) and unbiased estimators (9), a MF estimator of $\eta^{(1)}$ (denoting any of $\eta_k^{(1)}$'s) is defined as

$$\widehat{\eta}_{mf}^{(1)} = \overline{h(X^{(1)})}_{n_1} + \alpha(\overline{h(X^{(2)})}_{n_2} - \overline{h(X^{(2)})}_{n_1}) \quad (15)$$

$$= \alpha\overline{h(X^{(2)})}_{n_2} + (\overline{h(X^{(1)})}_{n_1} - \alpha\overline{h(X^{(2)})}_{n_1}) \quad (16)$$

where $\alpha \in \mathbb{R}$, e.g. Peherstorfer et al. [11]. This is an unbiased estimator by (9) since $\mathbb{E}\widehat{\eta}_{mf}^{(1)} = \eta^{(1)} + \alpha(\eta^{(2)} - \eta^{(2)}) = \eta^{(1)}$. The presence of α allows for potentially different scales of $h(X^{(1)})$ and $h(X^{(2)})$. When the outputs of the two codes are strongly dependent, the uncertainty associated with $\widehat{\eta}_{mf}^{(1)}$ is expected to be smaller than that of the baseline estimator,

$$\widehat{\eta}_{bl}^{(1)} = \overline{h(X^{(1)})}_{n_1}, \quad (17)$$

which is based on the high-fidelity data alone. This is because of the following two observations. First, if n_2 is much larger than n_1, the uncertainty associated with the first term of (16) is expected to be smaller since a larger sample is used. Second, if the outputs of the two codes are strongly dependent, the second term of (16) is expected to be on a smaller scale than (17), and hence have smaller uncertainty. That is,

$$\mathrm{Vrb}(\widehat{\eta}_{mf}^{(1)}) < \mathrm{Vrb}(\widehat{\eta}_{bl}^{(1)}), \quad (18)$$

where $\mathrm{Vrb}(\xi)$ denotes some measure of variability of the variable ξ; more on that below. Similarly, letting

$$\widehat{p}_{mf}^{(1)}(x_1^*),\ \widehat{p}_{bl}^{(1)}(x_1^*), \quad (19)$$

be the exceedance probability estimators of $p^{(1)}(x_1^*)$ through (5) for the estimators (15) and (17), respectively, Equation (18) translates into

$$\mathrm{Vrb}(\widehat{p}_{mf}^{(1)}(x_1^*)) < \mathrm{Vrb}(\widehat{p}_{bl}^{(1)}(x_1^*)). \quad (20)$$

The relations (18) and (20) are expected to translate into smaller confidence intervals for the respective quantities. The left-hand sides of (18) and (20) depend on the choice of α in (15). These could be minimized numerically over a range of α's.

What is taken for the measure(s) of variability in (18) and (20)? As $\widehat{\eta}_{mf}^{(1)}$ and $\widehat{\eta}_{bl}^{(1)}$ are moment estimators, the variance $\mathrm{Var}(\xi)$ seems a natural choice for (18). This implicitly assumes that the estimators are (asymptotically) normal so that their (normal) confidence interval can then be obtained as

$$(\widehat{\eta}_l^{(1)}, \widehat{\eta}_u^{(1)}) = \widehat{\eta}^{(1)} \pm c_\beta \widehat{\mathrm{Var}}(\widehat{\eta}^{(1)}), \quad (21)$$

where c_β is a critical value associated with a standard normal distribution and confidence level β (e.g. $c_\beta = 1.96$ for $\beta = 0.95$ or 95%). The difficulty in computing the variance and its estimate in (21) depends on the context. Having (21), the uncertainty can then be propagated onto $\widehat{p}^{(1)}(x_1^*)$, for example, through the boundary method (6) or another approach.

The variance as a measure of variability may not be convenient in other situations. For example, computing the variance of the estimators (14) for GEVD is challenging, especially when they are combined over two variables $X^{(1)}$ and $X^{(2)}$ as in (15). In such cases, the measure of variability is

$$\mathrm{Vrb}(\xi) = F_\xi^{-1}(\frac{1+\beta}{2}) - F_\xi^{-1}(\frac{1-\beta}{2}) \quad (22)$$

of a variable ξ, with $\beta \in (0,1)$ and CDF F_ξ of ξ (and its inverse F_ξ^{-1}). This measure represents the length of the $100\beta\%$ confidence interval for the population parameter that ξ estimates. The measure (22) could be estimated through non-parametric bootstrap. That is, in the case of $\widehat{\eta}_{mf}^{(1)}$, for example, B bootstrap samples $(X_{b,1}^{(1)}, X_{b,1}^{(2)}), \ldots, (X_{b,n_1}^{(1)}, X_{b,n_1}^{(2)})$, $b = 1, \ldots, B$, from $(X_i^{(1)}, X_i^{(2)})$, $i = 1, \ldots, n_1$, are obtained, and similarly $X_{b,n_1+1}^{(2)}, \ldots, X_{b,n_1+n_2}^{(2)}$, $b = 1, \ldots, B$, from $X_i^{(2)}$, $i = n_1 + 1, \ldots, n_1 + n_2$. These compute B bootstrap samples $\widehat{\eta}_{b,mf}^{(1)}$, $b = 1, \ldots, B$, of $\widehat{\eta}_{mf}^{(1)}$, and then also B bootstrap samples $\widehat{p}_{b,mf}^{(1)}(x_1^*)$, $b = 1, \ldots, B$. The latter data estimate $F_\xi^{-1}(\frac{1-\beta}{2})$ and $F_\xi^{-1}(\frac{1+\beta}{2})$ with $\xi = \widehat{p}_{mf}^{(1)}(x_1^*)$ in (22) through the empirical distribution of the bootstrap sample, and the confidence interval is set as

$$(\widehat{F}_\xi^{-1}(\frac{1-\beta}{2}), \widehat{F}_\xi^{-1}(\frac{1+\beta}{2})). \quad (23)$$

E.g., with $\beta = 0.95$, $\widehat{F}_\xi^{-1}(\frac{1-\beta}{2})$ is the 2.5% quantile of the bootstrap sample $\widehat{p}_{b,mf}^{(1)}(x_1^*)$, $b = 1, \ldots, B$. Similarly for $\widehat{\eta}_{bl}^{(1)}$ and $\widehat{p}_{bl}^{(1)}(x_1^*)$.

Illustrations of the discussed approach are given below.

Importance sampling

The setting considered here is motivated by the fact that in the ship application, both $X^{(1)}$ and $X^{(2)}$ depend on the same underlying (random) wave excitation. In LAMP and SC, the wave excitation is characterized through a set of deterministic frequencies and amplitudes, and a set of random phases, via the Longuett-Higgins wave model ((29) below). The random phases are determined by a random seed, which is just the record number in LAMP and SC. This means that for any value of $X^{(2)}$ from SC and the associated record number, the value of $X^{(1)}$ from LAMP could be obtained. This also means that many values of $X^{(2)}$ could be generated and examined first independently of $X^{(1)}$, since the former can be obtained efficiently. Then, if strong dependence is expected between $X^{(1)}$ and $X^{(2)}$, the high-fidelity code could be run to obtain the values of $X^{(1)}$ for larger values of $X^{(2)}$, hoping to get larger values of $X^{(1)}$ as a result. They could then evaluate $p^{(1)}(x_1^*)$ directly. The following discussion formalizes these ideas.

With the possibilities described above, an important observation explained next is that $X^{(2)}$ can be effectively sampled according to any proposal PDF $g^{(2)}(x_2)$, rather than the original PDF $f^{(2)}(x_2)$. By sampling from $g^{(2)}(x_2)$, an "actual" value of $X^{(2)}$ is sampled and the corresponding record number, so that its $X^{(1)}$ is generated. $X^{(2)}$ is assumed to have a bounded support (a,b). This will be revisited below. Since $X^{(2)}$ is associated with the lower-fidelity but computationally efficient code, a large sample $X^{(2)}_{n_1+1},\ldots,X^{(2)}_{n_1+n_2}$ of $X^{(2)}$ can be obtained by sampling from $f^{(2)}(x_2)$. For example, with SC, the current computational capabilities allow obtaining million of records in a matter of hours. Now, divide the range (a,b) into a large number M of subintervals of equal length (a_{m-1},a_m), $m=1,\ldots,M$, with $a=a_0<a_1<\ldots<a_M=b$. A reasonable number of points is assumed in each (a_{m-1},a_m). (The number of points will be larger in the subintervals where the PDF $f^{(2)}(x_2)$ is larger.) Next, to sample approximately from $g^{(2)}(x_2)$, follow these steps:

1. Set $p_m = C\,g^{(2)}(a_m)$, $m=1,\ldots,M$, with a constant C so that p_m's are probabilities with $\sum_{m=1}^M p_m = 1$;

2. Sample an index I from the set $\{1,\ldots,M\}$ according to the probabilities $\{p_1,\ldots,p_M\}$;

3. For $X^{(2)}$, pick at random a value from the set $\{X_i^{(2)} | X_i^{(2)} \in (a_{I-1},a_I), i=n_1+1,\ldots,n_1+n_2\}$.

Alternatively, in Step 3, $\xi^{(2)}$ from $g^{(2)}(x_2)$ is sampled, and $X^{(2)}$ is set as $X_i^{(2)}$ closest to $\xi^{(2)}$.

Example: For the PDF $g^{(2)}(x_2)$ which is uniform on (a,b), the probabilities $p_m = 1/M$ in Step 1 above. The procedure above then picks $X^{(2)}$ at random over the range (a,b).

If $X^{(2)}$ is sampled according to a proposal PDF $g^{(2)}(x_2)$, such sample $X_1^{(2)},\ldots,X_{n_1}^{(2)}$ is considered. Again, the sample is obtained from the PDF $g^{(2)}(x_2)$ as above, and not $f^{(2)}(x_2)$. Then, through the retained record numbers as noted above, the corresponding values $X_1^{(1)},\ldots,X_{n_1}^{(1)}$ can be generated. The pairs $(X_i^{(1)},X_i^{(2)})$ are obtained from the joint PDF $f(x_1|x_2)g^{(2)}(x_2)$, in contrast to the PDF $f(x_1|x_2)f^{(2)}(x_2)$ in the case of random sampling. (Here, $f(x_1|x_2)$ indicates the PDF of $X^{(1)}$ conditioned on $X^{(2)}=x_2$.) The importance sampling (IS) estimator of the exceedance probability $p^{(1)}(x_1^*)$ is now defined as

$$\widehat{p}_{is}^{(1)}(x_1^*) = \frac{1}{n_1}\sum_{i=1}^{n_1} 1_{\{X_i^{(1)}>x_1^*\}} w(X_i^{(2)}), \tag{24}$$

that is, as a weighted average of the occurrences of exceedances of interests (assuming now that these happen), where the importance sampling weights are

$$w(x_2) = \frac{f^{(2)}(x_2)}{g^{(2)}(x_2)}. \tag{25}$$

The motivation for the IS estimator (24) is that, with $\mathbb{E}_{g^{(2)}}$ indicating the expectation with respect to $g^{(2)}$,

$$\begin{aligned}\mathbb{E}\widehat{p}_{is}^{(1)}(x_1^*) &= \mathbb{E}_{g^{(2)}}(1_{\{X^{(1)}>x_1^*\}} w(X^{(2)})) \\ &= \int\int 1_{\{x_1>x_1^*\}} w(x_2) f(x_1|x_2) g^{(2)}(x_2) dx_1 dx_2 \\ &= \int\int 1_{\{x_1>x_1^*\}} f(x_1|x_2) f^{(2)}(x_2) dx_1 dx_2 \\ &= \int 1_{\{x_1>x_1^*\}} f^{(1)}(x_1) dx_1 = p^{(1)}(x_1^*). \end{aligned} \tag{26}$$

This argument assumes that the support of $g^{(2)}$ and $f^{(2)}$ coincide. Similarly,

$$\mathrm{Var}(\widehat{p}_{is}^{(1)}(x_1^*)) = \frac{\mathbb{E}(1_{\{X^{(1)}>x_1^*\}} w(X^{(2)})^2) - p^{(1)}(x_1^*)^2}{n_1}. \tag{27}$$

The variance can be estimated through weighted averages as (24), and used in a normal confidence interval around $\widehat{p}_{is}^{(1)}(x_1^*)$.

Remark: In O'Connor et al. [10], estimation of the whole PDF $f^{(1)}(x_1)$ is considered and a uniform proposal PDF $g^{(2)}(x_2)$ is generally suggested to use for the whole range. The IS approach is also compared in that work to Gaussian process regression, which is another method for the considered problem.

Following the remark, a uniform proposal PDF $g^{(2)}(x_2)$ shall be taken, The case of strong dependence could do better by sampling more frequently around x_2^* for which $X^{(1)}$ lies around x_1^* (e.g., sampling more frequently

around $x_2^* = 8$ in Figure 6 below for the considered illustration).

Example: For the PDF $g^{(2)}(x_2)$ which is uniform on (a,b), the IS estimator (24) simplifies to

$$\widehat{p}_{is}^{(1)}(x_1^*) = \frac{b-a}{n_1}\sum_{i=1}^{n_1} 1_{\{X_i^{(1)}>x_1^*\}} f^{(2)}(X_i^{(2)}). \qquad (28)$$

This estimator will serve conveniently to make a few points below.

Illustrations of the discussed approach are given below, where the importance and random sampling approaches shall be compared. One key difference is that while a parametric PDF is used with random sampling, the IS approach is largely nonparametric. The IS method may also be more flexible to estimate $p^{(1)}(x_1^*)$ for a range of x_1^*'s.

Numerical illustrations

To illustrate the MFUQ methods, the flared geometry is considered in the conditions described above (head seas, sea state 8, and so on). Heave motion and its minima over 30-minute records of LAMP and SC are discussed. The sign of the minima is changed throughout so that large negative minima correspond to large positive values (referred to as absolute minima below). Heave and its extremes are of interest because of, e.g., their connections to heave accelerations and relative motion. To explain the methods is the goal, rather than to find the most useful application.

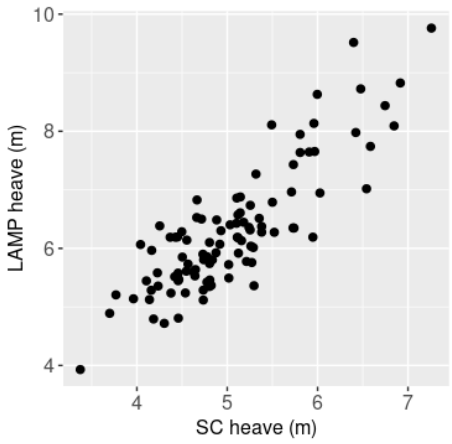

Figure 3: Heave record (absolute) minima: LAMP versus SC for 100 randomly selected records.

First, the case of random sampling is discussed. Figure 3 depicts the heave record (absolute) minima for LAMP versus SC over 100 randomly selected records. The scatter plot shows a fairly strong dependence between the LAMP and SC record minima. (The vertical axis refers to $X^{(1)}$, and the horizontal axis to $X^{(2)}$.) For MF estimation, additional 2,000 SC records are employed.

As record extreme values are considered, the LAMP PDF can be modeled as a GEVD. From above, the GEVD is characterized by the first three L-moments (12). Does the strong dependence translate into smaller variability of the MF estimators of these moments, as expressed through Eq. (18)? The variability is measured through the quantity (22), and it is estimated through bootstrap. The boxplots of bootstrapped first three L-moments for baseline (BL) and multifidelity (MF) estimators are presented in Figure 4. From the figure, the MF moment estimators have smaller variability, especially so for the first and second L-moments.

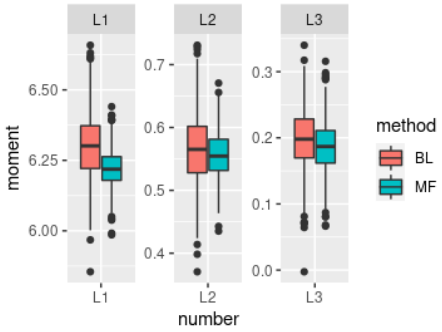

Figure 4: Boxplots of bootstrapped first three L-moments for baseline (BL) and multifidelity (MF) estimators.

The smaller variability of the MF moment estimators propagates into a smaller variability of the MF estimator of the exceedance probability. This is seen in Figure 5 for the exceedance probability with the critical value $x_1^* = 10$ (m). The choice of this critical value is driven by two considerations: first, none of 100 LAMP record minima observations are above this value as seen from Figure 3, and second, the value is also taken in connection to the comparison to the IS approach below. The left plot of Figure 5 shows similarly the boxplots of the bootstrapped exceedance probability estimates resulting from the BL and MF estimators of L-moments. The right plot of Figure 5 is the resulting confidence intervals, computed as the 2.5% and 97.5% quantiles of the bootstrap values. The points inside the intervals indicate the actual estimates of the exceedance probability. To reiterate the main point, the MF confidence interval is smaller than the BL confidence interval.

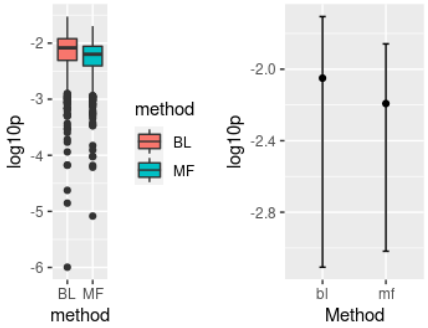

Figure 5: Left: Boxplots of resulting bootstrapped exceedance probability estimates for BL and MF approaches. Right: Corresponding confidence intervals.

The importance sampling approach is now described. Here, $100,000$ SC records are generated, and their record heave (absolute) minima are documented. Except 10 extreme values, the (absolute) minima fall in the interval $(3.2, 9)$. This interval is discretized into subintervals of size 0.1 to sample SC records uniformly. The few observations below 3.2 and above 9, are considered artificially to belong to the subintervals $(3.1, 3.2)$ and $(9, 9.1)$ for sampling purposes. (A remark below is stated for a further discussion on the latter step.) Then, 290 SC records are sampled uniformly from the interval $(3.1, 9.2)$ of their minima values. For each of the sampled values, LAMP is run for the corresponding record number, and the corresponding LAMP record minima are obtained. The scatter plot of the resulting 290 pairs of LAMP and SC record heave (absolute) minima is depicted in Figure 6.

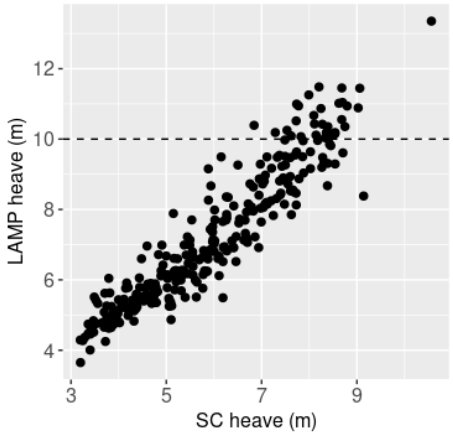

Figure 6: Heave record (absolute) minima: LAMP versus SC for 290 SC records from importance sampling.

Comparing Figures 6 and 3, the former now has larger LAMP values, in particular and in contrast to the latter, a number of observations above the critical value $x_1^* = 10$ (m). The resulting importance sampling (IS) confidence interval for the probability exceeding this critical value is in Figure 7, along the same BL and MF confidence intervals from the right plot of Figure 5. The IS estimator gives a slightly smaller estimate of the exceedance probability. This could result from the actual PDF of LAMP deviating in the tail from the PDF fitted based on a random sample. The IS approach is inherently more flexible in capturing such model PDF misspecification if it occurs.

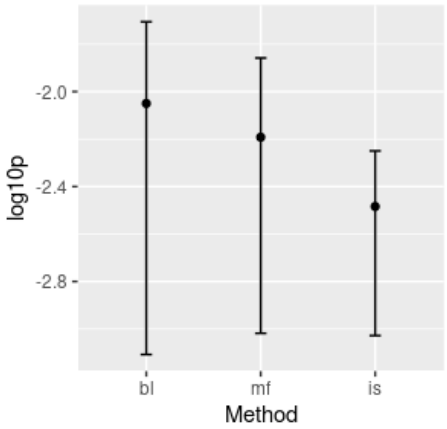

Figure 7: Confidence intervals for exceedance probability: BL and MF as in Fig. 5, and IS obtained from the importance sampling approach.

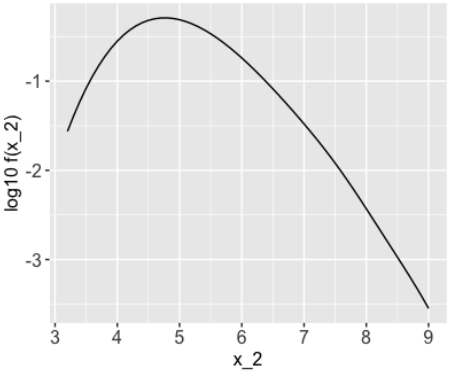

Figure 8: The kernel smoothing density estimate of $f^{(2)}(x_2)$.

Remark: The assumption of the finite support $(3.2, 9)$ (or $(3.1, 9.1)$ after a slight enlargement) considered for $X^{(2)}$ above is discussed. The PDF of $X^{(2)}$ estimated through kernel smoothing on $(3.2, 9)$ is depicted in Figure 8. The value of the density at $x_2 = 9$ is around $10^{-3.5}$. Assuming they all lead to $X^{(1)} > x_1^* = 10$, the contribution to (28) of m (≤ 10 as noted above) points

above $x_2 = 9$ is smaller than

$$\frac{b-a}{n_1}10^{-3.5}m \leq \frac{9-3.2}{290}10^{-3.5}10 \simeq 6\cdot 10^{-5}.$$

This will not affect significantly the IS estimator and confidence intervals reported in Figure 7.

For the IS approach to work, the outputs of LAMP and SC need to be strongly dependent, as in Figure 6. This may not always be the case. For example, Figure 9 depicts an analogous scatter plot in the same conditions obtained similarly through the IS approach but for LAMP and SC loads, namely, the vertical bending moment (VBM) at midship. Larger values of LAMP VBM now may as well result from smaller values of SC VBM, making the IS procedure less beneficial. The LSTM approach considered below will map SC VBM to outputs matching LAMP VBM considerably better (Figure 21), so that the IS approach is promising to use again.

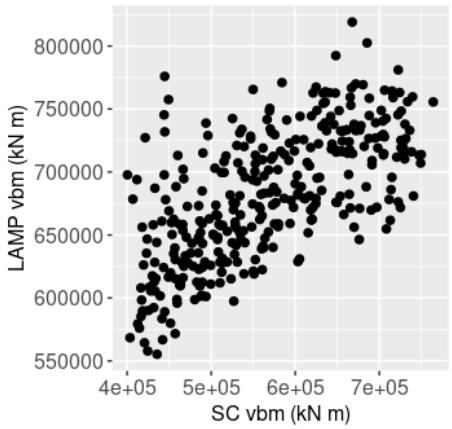

Figure 9: VBM record maxima: LAMP versus SC for 347 SC records from importance sampling.

REDUCED-ORDER MODELING AND EXTREMES

The MFUQ methods considered above are superior to baseline estimation when LAMP and SC produce strongly dependent outputs at extremes. To calibrate the outputs better, two approaches below are considered with illustrations.

Regression approach: description

The setting and the notation of head seas described following (1) and the focus on heave ζ_g and pitch θ are continued. The common Longuett-Higgins wave elevation form is given (in head seas) by

$$\sum_{n=1}^{N_w} a_{w_n}\cos(k_{w_n}x - \omega_{w_n}t + \varphi_{0,n}) \tag{29}$$

for a set of deterministic discrete frequencies ω_{w_n}, their wave numbers k_{w_n}, deterministic amplitudes a_{w_n} and random phases $\varphi_{0,n}$. The random seed or the record number determines the random phases used for a given record.

The regression approach has the following goals. To choose the added mass coefficients A_{ij} and damping coefficients B_{ij} $(i,j = 3,5)$ accounting for the radiation forces in LAMP as

$$F_{i,rad} \simeq A_{i3}\ddot{\zeta}_g + A_{i5}\ddot{\theta} + B_{i3}\dot{\zeta}_g + B_{i5}\dot{\theta} \tag{30}$$

is one goal. To capture the diffraction and FKHS forces in LAMP is another goal. Letting $F_{i\cdot}$ denote either $F_{i,fkhs}$ or $F_{i,dif}$,

$$F_{i\cdot}(t) = \sum_{n=1}^{N_w} F_{i\cdot,n}\cos(\omega_{w_n}t + \gamma_{i\cdot,n} + \varphi_{0,n}), \tag{31}$$

where the amplitudes $F_{i\cdot,n}$ and phases $\gamma_{i\cdot,n}$ form a collection of (deterministic) additional frequency-dependent coefficients to set.

To calculate the coefficients A_{ij}, B_{ij}, the LAMP option is performed for the forced motion calculations, resulting in hydrodynamic forces that incorporate radiation only but not diffraction. More specifically, two additional LAMP calculations are executed: a forced heave LAMP run and a forced pitch LAMP run. In a forced heave run, the heave motion from the original LAMP run is forced in calm water, resulting in heave and pitch radiation forces F_{33} and F_{53}, respectively. Similarly, a forced pitch run results in heave and pitch radiation forces F_{35} and F_{55}, respectively. Letting $Y \sim aX$ denote a regression operation of Y on X with a regression coefficient a, the coefficients A_{ij}, B_{ij} are then obtained from the regressions

$$\begin{aligned} F_{33} &\sim A_{33}\ddot{\zeta}_g + B_{33}\dot{\zeta}_g \\ F_{53} &\sim A_{53}\ddot{\zeta}_g + B_{53}\dot{\zeta}_g \end{aligned} \tag{32}$$

and

$$\begin{aligned} F_{35} &\sim A_{35}\ddot{\theta} + B_{35}\dot{\theta} \\ F_{55} &\sim A_{55}\ddot{\theta} + B_{55}\dot{\theta}. \end{aligned} \tag{33}$$

The coefficients in these regressions depend on the considered frequencies, and as explained below, a more refined analysis is undertaken for multiple frequencies.

To calculate the frequency dependent coefficients $F_{i,dif,n}$ and $\gamma_{i,dif,n}$ in the diffraction forces, another LAMP option is selected allowing fixed-body (wave pass) calculations, for which hydrodynamic forces now incorporate only diffration. This is a fixed-body LAMP run, resulting in the heave and pitch diffraction forces $F_{3,dif}$ and $F_{5,dif}$, respectively. Then, in view of

Equation (31),

$$F_{i,dif}(t) \sim \sum_{n=1}^{N_w} F_{c,i,n}\cos(\omega_{w_n}t+\varphi_{0,n}) + F_{s,i,n}\sin(\omega_{w_n}t+\varphi_{0,n}) \tag{34}$$

and the frequency-dependent coefficients of interest are set as $F_{i,dif,n} = \sqrt{F_{c,i,n}^2+F_{s,i,n}^2}$ and $\gamma_{i,dif,n} = \arctan(-F_{s,i,n}/F_{c,i,n})$.

However, one important caveat exists with the regression (34). When the number of frequencies N_w is large (say, 100), the regression (34) has a large number of parameters and their estimates are quite unstable. In that case, a penalized regression is run forcing the cosine and sine coefficients to vary smoothly over the range of frequencies. The penalized regression works as follows. Collecting the data and coefficients into vectors and matrices

$$Y = \begin{pmatrix} F_{i,dif}(t_1) \\ \vdots \\ F_{i,dif}(t_N) \end{pmatrix}_{N\times 1}, \eta = \begin{pmatrix} (F_{c,i,n})_{n=1,\ldots,N_w} \\ (F_{s,i,n})_{n=1,\ldots,N_w} \end{pmatrix}_{2N_w\times 1}, \tag{35}$$

$$X = \begin{pmatrix} (\cos(\omega_{w_n}t_k+\varphi_{0,n}))_{n=1,\ldots,N_w,k=1,\ldots,N}, \\ (\sin(\omega_{w_n}t_k+\varphi_{0,n}))_{n=1,\ldots,N_w,k=1,\ldots,N} \end{pmatrix}_{N\times 2N_w}, \tag{36}$$

the standard regression problem for η minimizes $\|Y - X\eta\|_2^2$, where $\|\cdot\|_2$ denotes the Euclidean norm. The penalized regression for η, on the other hand, minimizes

$$\|Y - X\eta\|_2^2 + \lambda\|\mathscr{D}\eta\|_2^2. \tag{37}$$

Here, $\lambda > 0$ is a penalty parameter and the matrix $\mathscr{D}$ is a block matrix

$$\mathscr{D} = \begin{pmatrix} D & 0_{N_w\times(N_w-2)} \\ 0_{N_w\times(N_w-2)} & D \end{pmatrix} \tag{38}$$

with $0_{p\times q}$ indicating a $p\times q$ matrix of zeros, and

$$D = \begin{pmatrix} 1 & -2 & 1 & 0 & \ldots & 0 & 0 & 0 \\ 0 & 1 & -2 & 1 & \ldots & 0 & 0 & 0 \\ \vdots & \vdots & \vdots & \vdots & \ddots & \vdots & \vdots & \vdots \\ 0 & 0 & 0 & 0 & \ldots & 1 & -2 & 1 \end{pmatrix}. \tag{39}$$

When applied to η, the matrix $\mathscr{D}$ computes second-order differences (over adjacent frequencies) of the cosine and sine coefficients, and the penalty $\lambda\|\mathscr{D}\eta\|_2^2$ forces these differences to be smaller, and thus the coefficients to vary smoothly over the range of frequencies. Illustrations of this are given below. The solution to minimizing (37) can be written explicitly as

$$\widehat{\eta} = (X'X + \lambda\mathscr{D}'\mathscr{D})^{-1}X'Y. \tag{40}$$

Finally, to calculate the frequency dependent coefficients in the FKHS forces, an approach is followed similar to that for the diffraction above. But as noted above, simplifying FHKS forces is not critical to reduced order models.

Regression approach: illustrations

The regression approach described above is illustrated in several scenarios. LAMP-1 calculations are employed, and as a reduced-order model, the ODE system (3) is taken, where the FKHS forces are separated into HS and FK components (a reasonable assumption for smaller waves), and where the diffraction forces are added to the motion equations. In the way the FKHS forces are computed, this is a slightly simpler model than SC. But to manage for illustration purposes is easier here. The regression approach is currently still transitioning to SC, which is a much more elaborate code.

The two models, LAMP-1 and reduced-order, were compared for regular waves in Pipiras et al. [12] where the regression captured nearly perfectly the various forces and led to heave and pitch motions from the reduced-order model that are nearly identical to those from LAMP-1. Here, the cases of bi-chromatic waves (i.e., $N_w = 2$ in (29)) and irregular waves (i.e., $N_w = 120$) are evaluated. The irregular waves, in particular, correspond to sea state 5, with the significant wave height of 3.26 m and the modal period of 9.7 sec.

Radiation forces: Whereas regression captures perfectly the various forces in regular waves, this is not expected when the number of frequencies N_w in (29) increases. Indeed, the resulting added mass and damping coefficients A_{ij}, B_{ij} in (3) are well known to depend on frequency. This can already be observed, for example, from Figure 10 that depicts the LAMP radiation force F_{33} in heave (and forced heave run) over a time window, and the force resulting from the regression (32) in bi-chromatic waves. A small discrepancy occurs between the two.

The discrepancy is more pronounced in the case of irregular waves, as depicted in Figure 11 through the dotted line. In fact, in this case, the regression (32) produces a negative damping coefficient, which results in unstable (diverging) motions of the reduced-order model. To overcome this issue, the spectrum of the force F_{33} is computed, and the frequency is identified where the spectrum is largest. The forced motion calculation is rerun for that maximum frequency, and the regression coefficients are recaluculated. The resulting force for that

rerun regression is depicted in the same Figure 11 but in dashed line. The maximum frequency depends only slightly on a given record number (random seed).

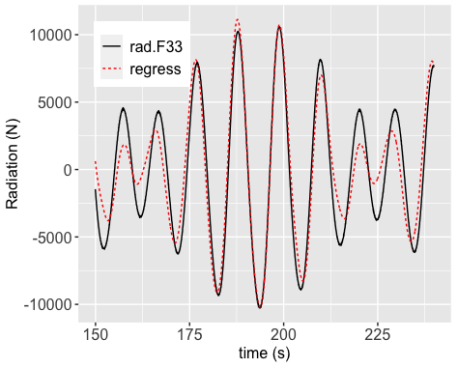

Figure 10: The radiation force F_{33} and its regression approximation for bi-chromatic waves.

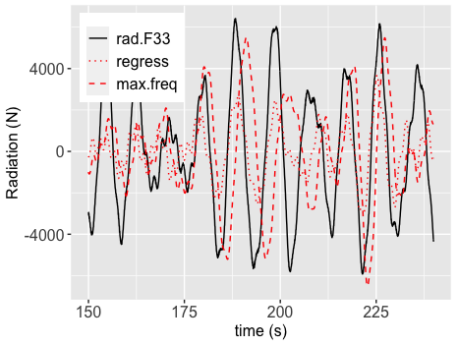

Figure 11: The radiation force F_{33} and its regression approximations for irregular waves.

Diffraction forces: The need and results for the penalized regression following (34) are described. Figure 12 depicts the cosine coefficients $F_{c,3,n}$ in (34) over the frequency range index n resulting from the penalized regression for several records (labeled "rec1" and "rec2" in the legend) and several values of the penalty parameter λ. For a small value of $\lambda = 10$ (label "rec1.small"), the coefficient estimates are quite unstable. In fact, the matrix $X'X + \lambda \mathscr{D}'\mathscr{D}$ in (40) is numerically singular for $\lambda = 0$, corresponding to the standard least squares estimator. For $\lambda = 10^5$ (labels "rec1.large" and "rec2.large"), the coefficient estimates vary much smoother over the frequency index range. Furthermore, the estimates are very close across the two chosen records.

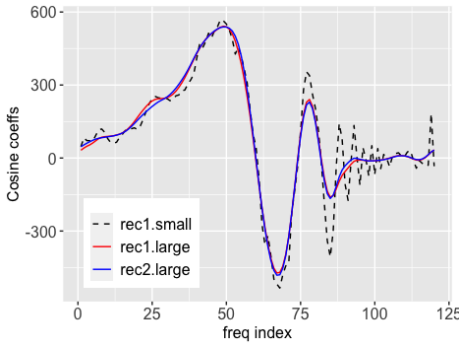

Figure 12: The cosine coefficients $F_{c,3,n}$ over the frequency index n for the diffraction force $F_{3,dif}$.

Motions and extremes: The estimated regression coefficients enter into the reduced-order model, resulting in heave and pitch motions. Figure 13 depicts (centered) heave motions over a time window for LAMP and the reduced-order model for irregular waves. The heave motion produced by an ad hoc choice of the added mass and damping coefficients, and without diffraction forces also appears in the plot.

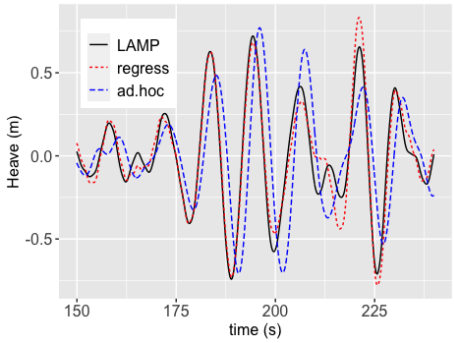

Figure 13: The heave motions for LAMP, and the regression-based and ad-hoc reduced-order models for irregular waves.

A notable feature of the motions produced by the regression-based reduced-order model, when compared to the ad-hoc approach, is a much better agreement in phase. This translates into a better agreement in extremes as well, as illustrated through Figures 14 and 15. Figure 14 depicts the scatter plot of heave peaks over a certain threshold for LAMP versus regression-based and ad-hoc reduced-order models for one record (of 500 second length). The peaks are more strongly dependent for the regression approach. E.g. the correlation coefficients are 0.85 and 0.68 for the two approaches. Figure 15 depicts the scatter plot of heave record maxima for LAMP versus regression-based and ad-hoc reduced-order models for 15 records. The correlation coefficients here are 0.87 and 0.59 for the two

approaches. The results for pitch motions and forces are similar and not reported here.

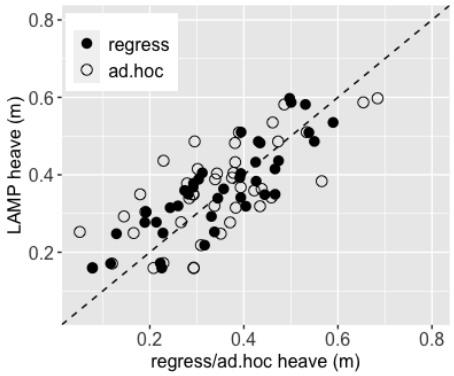

Figure 14: The peaks of LAMP versus regression-based and ad-hoc reduced-order models.

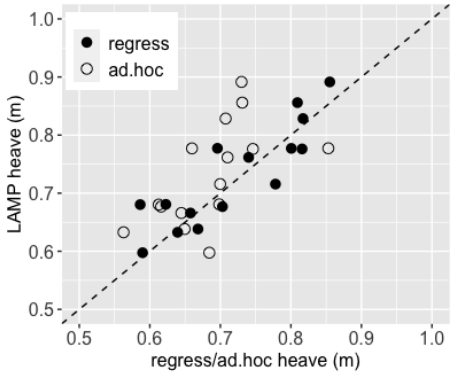

Figure 15: The record heave maxima of LAMP versus regression-based and ad-hoc reduced-order models.

In conclusion, the regression-based reduced-order model leads overall to stronger dependence in extremes and hence the likelier benefits of the MFUQ methods.

LSTM approach: description

To calibrate SC to LAMP by long short term memory (LSTM) neural networks (Hochreiter and Schmidhube [6]) is reported here. In the case of motions, a trained LSTM network takes SC heave, pitch and roll motions, and the wave elevation at the center of gravity, and maps them in a computationally efficient manner to LAMP heave, pitch and roll motions. In the case of VBM in head seas, SC heave, pitch, wave elevation and VBM are predictors for LAMP VBM. In fact, removing any of the considered predictors deteriorates the results.

The training (and validation) is performed on a number of records for the same sea state, heading and other conditions. Time history data are sub-sampled to a 1 second interval for this purpose. The LSTM architecture consists of 2 layers and a hidden state size of 30. With MSE referring to Mean Squared Error, and y_L and y_S to LAMP and SC signals, respectively, several objective functions are tried as:

- MSE: $\frac{1}{N}\sum_i (y_L(t_i) - y_S(t_i))^2$
- Peak amplitude MSE (pMSE):

$$\frac{1}{N} \sum_{i\,:\,t_i \text{ is LAMP peak}} (y_L(t_i) - y_S(t_i))^2$$

More detailed description of the LSTM approach can be found in Levine et al. [8], where the approach has also been tried successfully across different conditions. The performance of the LSTM model for extremes is the focus here. The questions of interest are: Does the LSTM model perform well for extremes? Does the choice of the objective function above affect performance? Should training be carried out on records with extreme behavior?

LSTM approach: illustrations

Before illustrating the full potential of the LSTM model, the results reported in Figure 15 are reviewed. Ten (10) records of the ad-hoc reduced-order model train (and validate) an LSTM model, and the other 5 records test it. The resulting outputs are depicted in Figure 16, with the same outputs for the regression-based model as in Figure 15. The LSTM approach leads to a slightly better match to LAMP outputs.

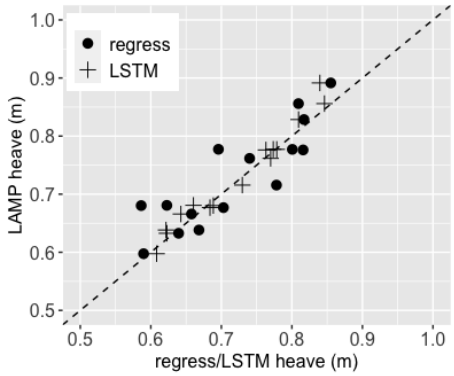

Figure 16: The record heave maxima of LAMP versus regression-based and LSTM models.

The LSTM approach, however, is more universal in its applicability and produces very promising results in the application. This is illustrated on a few scenarios, also answering the questions raised above. Figures 17 and 18 show LSTM performance for the ship in beam seas (90 deg heading), with the seas state 8 and zero speed. The LSTM was trained on 50 SC records, and the model

performance is reported for another set of 50 SC records. Similar scatter plots of record maxima compare extreme behavior. The results are included for roll and heave motions only. Furthermore, the LSTM outputs are given for both MSE and pMSE objective functions. In these experiments, the pMSE objective function led to a slightly better match of LSTM outputs to LAMP, for example, for larger values in Figure 18. But the overall improvement was small. Similarly, not much benefit was found of training an LSTM on records with extreme observations. Independently of how the training was executed, from Figures 17 and 18, the LSTM outputs align much closer to the LAMP outputs than the SC outputs.

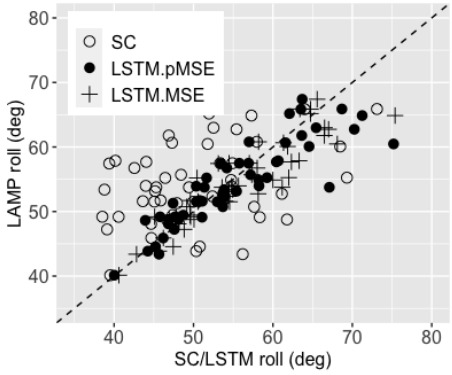

Figure 17: The record roll maxima of LAMP versus LSTM models in beam seas.

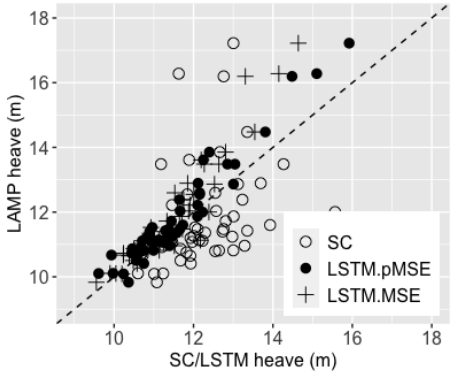

Figure 18: The record heave maxima of LAMP versus LSTM models in beam seas.

Figures 19 and 20 indicate similar scatter plots for pitch and heave but in head seas, in the same conditions in the illustrations of the MFUQ methods above. The results are for the pMSE objective function only. Once again, the LSTM approach performs very well for extremes.

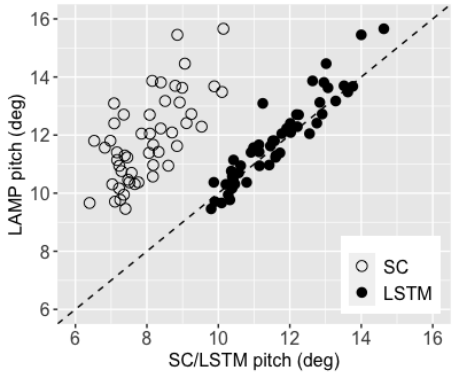

Figure 19: The record pitch maxima of LAMP versus LSTM models in head seas.

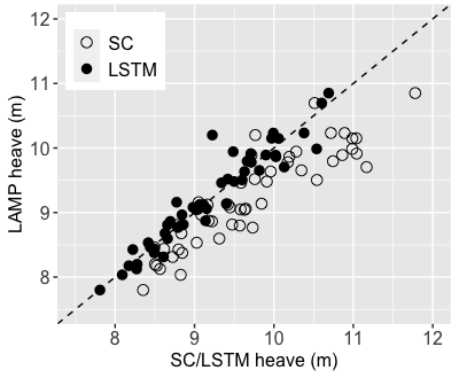

Figure 20: The record heave maxima of LAMP versus LSTM models in head seas.

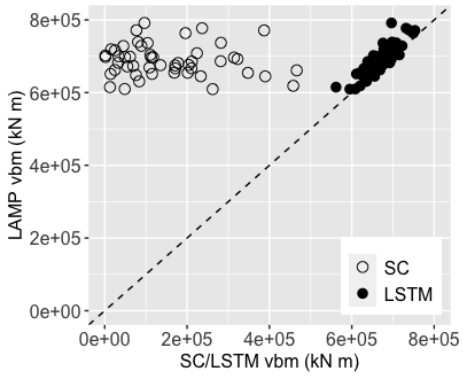

Figure 21: The record VBM maxima of LAMP versus LSTM models in head seas.

Finally, Figure 21 is for VBM at midship, where the performance of LSTM is even more striking. This plot complements the discusion around Figure 9. Altogether, LSTM models perform very well and hold great promise

for the considered MFUQ methods for extreme motions and loads.

CONCLUSION

Several methods for uncertainty quantification (UQ) are presented when estimating extreme quantities in multi-fidelity (MF) setting. In the application to ship motions and loads, several computer codes (LAMP and SimpleCode, in particular) played the role of MF sources, for which several methods were examined, both physics-informed (regression of forces) and data-driven (LSTM), for better calibration at the extremes. The feasibility and promise of the proposed approaches were demonstrated, but they are yet to be integrated fully into the current capabilities of the ship motion codes. For example, the option to incorporate diffraction forces into SimpleCode through frequency dependent coefficients is currently being implemented. Adding the trained LSTM model to SimpleCode so that the corrected motions, loads, extremes and other quantities could readily be outputted is another task left for the near future.

ACKNOWLEDGEMENTS

This work was funded by the Office of Naval Research (ONR) under Dr. Woei-Min Lin. Dayne Howard's graduate thesis work supporting this paper was funded by the Department of the Navy as part of his enrollment in the Naval Construction and Engineering graduate program (Course 2N) at Massachusetts Institute of Technology. The participation of Profs. Pipiras and Sapsis was also facilitated by the NSWCCD Summer Faculty Program, managed by Dr. Jack Price. The authors are very grateful for the support that made this work possible.

REFERENCES

Belenky, V. L., Pipiras, V., Weems, K. and Sapsis, T., "Volume-based approach to extreme properties of vertical bending moment," Proceedings of the 34th Symposium on Naval Hydrodynamics, Washington, DC, 2022.

Bishop, R., Belknap, W., Turner, C., Simon, B. and Kim, J., "Parametric investigation on the influence of GM, roll damping, and above-water form on the roll response of model 5613," Technical report, NSWCCD-50-TR-2005/027, Hydromechanics Department, Naval Warfare Center Carderock Division, West Bethesda, Maryland, 2005.

Brown, B. and Pipiras, V., "Multifidelity Monte Carlo estimation for extremes through extrapolation distributions," Preprint available at https://pipiras.web.unc.edu/papers/, 2022.

Coles, S., An Introduction to Statistical Modeling of Extreme Values, Springer Series in Statistics, Springer-Verlag London Ltd., 2001.

Glotzer, D., Pipiras, V., Belenky, V. L., Campbell, B. and Smith, T., "Confidence intervals for exceedance probabilities with application to extreme ship motions," REVSTAT Statistical Journal, Vol. 15, 2017, pp. 537–563.

Hochreiter, S. and Schmidhuber, J., "Long short-term memory," Neural Computation, Vol. 9, 1997, pp. 1735–1780.

Hosking, J. R. M., Wallis, J. R., and Wood, E. F., "Estimation of the generalized extreme-value distribution by the method of probability-weighted moments," Technometrics, Vol. 27, 1985, pp. 251–261.

Levine, M. D., Edwards, S. J., Belenky, V. L., Weems, K., Howard, D., Sapsis, T., and Pipiras, V., "Data-adaptive autonomous seakeeping," Proceedings of the 34th Symposium on Naval Hydrodynamics, Washington, DC, 2022.

Lin, W. M. and Yu, D. K. P., "Numerical solutions for large amplitude ship motions in the time-domain," Proceedings of the 18th Symposium on Naval Hydrodynamics, Ann Arbor, 1991.

O'Connor, K., Pipiras, V. and Sapsis, T., "Sampling low-fidelity outputs for high-fidelity density estimation," Preprint available at https://pipiras.web.unc.edu/papers/, 2022.

Peherstorfer, B., Willcox, K. and Gunzburger, M., "Optimal model management for multifidelity Monte Carlo estimation," SIAM Journal on Scientific Computing, Vol. 38, 2016, pp. A3163–A3194.

Pipiras, V., Belenky, V. L., Weems, K., Brown, B., Frommer, A. and Ouimette, G., "Calibrating multifidelity ship motion codes through regression," Proceedings of the 1st International Conference on the Stability and Safety of Ships and Ocean Vehicles, Glasgow, Scotland, UK, 2021.

Sapsis, T., Belenky, V. L., Weems, K. and Pipiras, V., "Deck effects on the statistical structure of the vertical bending moment loads during random waves: an analytical treatment ," Proceedings of the 34th Symposium on Naval Hydrodynamics, Washington, DC, 2022.

Shin, Y. S., Belenky, V. L., Lin, W. M., Weems, K. M. and Engle, A. H., "Nonlinear time domain simulation technology for seakeeping and wave-load analysis for modern ship design. Authors' closure," Transactions os

the Society of Naval Architects and Marine Engineers, Vol. 111, 2003, pp. 557–583.

Weems, K., Belenky, V. L., Spyrou, K., Aram, S. and Silva, K., "Towards numerical estimation of probability of capsizing caused by broaching-to," Proceedings of the 18th Symposium on Naval Hydrodynamics, Osaka, Japan, 2020.

Weems, K., Lin, W.-M., Zhang, S., Meinhold, M. J., Weems, M. H. and others, Large Amplitude Motion Program (LAMP) for Ship Motions and Wave Loads Predictions, Version 4.0.9, Leidos Corporation, Bowie, MD, 2019.

Weems, K. and Wundrow, D., "Hybrid models for fast time-domain simulation of stability failures in irregular waves with volume-based calculations for Froude-Krylov and hydrostatic forces," Proceedings of the 13th International Ship Stability Workshop, Brest, France, 2013.